Release of Photoactivatable Drugs from Plasmonic Nanoparticles for Targeted Cancer Therapy

Yun-Ling Luo, Yi-Syun Shiao, and Yu-Fen Huang*

Department of Biomedical Engineering and Environmental Sciences, National Tsing Hua University, Hsinchu, Taiwan, Republic of China

ABSTRACT Chemotherapy is an important modality in cancer treatment. The major challenges of recent works are to improve drug loading, increase selectivity to target cells, and control the precise release of drugs. In the present study, we devised a smart drug carrier, an aptamer/hairpin DNA—gold nanoparticle (apt/hp-Au NP) conjugate for targeted delivery of drugs. The DNA aptamer sgc8c, which possesses strong affinity for protein tyrosine kinase 7 (PTK7), abundantly expressed on the surface of CCRF-CEM (T-cell acute lymphoblastic leukemia) cells, was assembled onto the surface of Au NPs. The repeated d(CGATCG) sequence within the hpDNA on the Au NP surface was used for the loading of the anticancer drug doxorubicin (Dox). After optimization, 25 (±3) sgc8c and 305 (±9) Dox molecules were successfully loaded onto the AuNP (13 nm) surface. The binding capability of apt/hp-Au NP conjugates toward targeted cells was investigated by flow cytometry and atomic absorption spectroscopy, which showed that the aptamer-functionalized nanoconjugates were selective for targeting of cancer cells. A cell toxicity (3-(4,5-dimethylthiazol-2-yl)-5-(3-carboxymethoxyphenyl)-2-(4-sulfophenyl)-2*H*-tetrazolium, MTT) assay also demonstrated that these drug-loaded nanoconjugates could kill targeted cancer cells more effectively than nontargeted (control) cells. Most importantly, when illuminated with plasmon-resonant light (532 nm), Dox:nanoconjugates displayed enhanced antitumor efficacy with few side effects. The marked release of Dox from these nanoconjugates in living cells was monitored by increasing fluorescence signals upon light exposure. *In vitro* studies confirmed that aptamer-functionalized hp-Au NPs can be used as carriers for targeted delivery of drugs with remote control capability by laser irradiation with high spatial/temporal resolution.

KEYWORDS: aptamer · gold nanoparticle · controlled drug release · targeted cancer therapy · photothermal effect

Strategies for controlled pharmaceutical release have been actively studied for applications in drug delivery,[1,2] gene therapy,[3−5] and tissue engineering.[6,7] External stimuli such as temperature,[8−11] pH,[12−14] ionic strength,[15,16] redox reagents,[17] and enzymes[18−21] are particularly important factors that can induce a physicochemical change of "smart" vehicles and, in turn, enable the precise delivery of guest molecules to target sites. For instance, hydrogels that undergo a conformational change (*i.e.*, swelling/deswelling) triggered by pH variations are commonly utilized to release encapsulated drugs when passing through a region of low pH (pH 5−7).[22−25] However, release mechanisms based on specific changes in the surrounding medium may cause unpredictable payload release to various cellular locations and cell types. A finely responsive system that is sensitive to subtle environmental variations remains a major challenge. Therefore, triggers that can be controlled exogenously by irradiation with light or by exposure to electrical and magnetic fields are becoming increasingly attractive.[26−33] In addition to an external property that can be activated, remote control also enables the intracellular release process with remarkable spatial/temporal resolution.

Recent advances in the development of plasmonic nanoparticles (NPs) have presented new opportunities for controllable drug release. These metallic NPs possess intense collective plasmonic resonance and extremely low quantum yield; the absorbed photon energy is converted into heat with high efficiency upon optical illumination.[34,35] The heat rapidly dissipated into the surroundings has been utilized to trigger the release of preloaded effectors. For clinical applications, gold NPs (Au NPs) are known to be less cytotoxic in comparison with other inorganic nanomaterials.[36−40] Au NPs are chemically inert and are easy to synthesize and manipulate with a wide variety of guest molecules. A high surface-to-volume ratio[41−44] and/or hollow structure[45] also help them to serve as novel delivery carriers. More importantly, their geometrically tunable optical characteristics and their strong photothermal response suggest the great potential of Au NPs for facilitating light-triggered gene/drug release in a nondestructive and controlled manner.[46−53]

The results mentioned above are an excellent motivation for designing a new drug release system based on Au NPs. Here, we used Au NPs as a nanoplatform to assemble multiple copies of hairpin DNA (hpDNA). With precisely controllable density and covalent conjugation, the binding of

* Address correspondence to yufen@mx.nthu.edu.tw.

Received for review May 1, 2011 and accepted September 26, 2011.

Published online September 26, 2011
10.1021/nn201592s

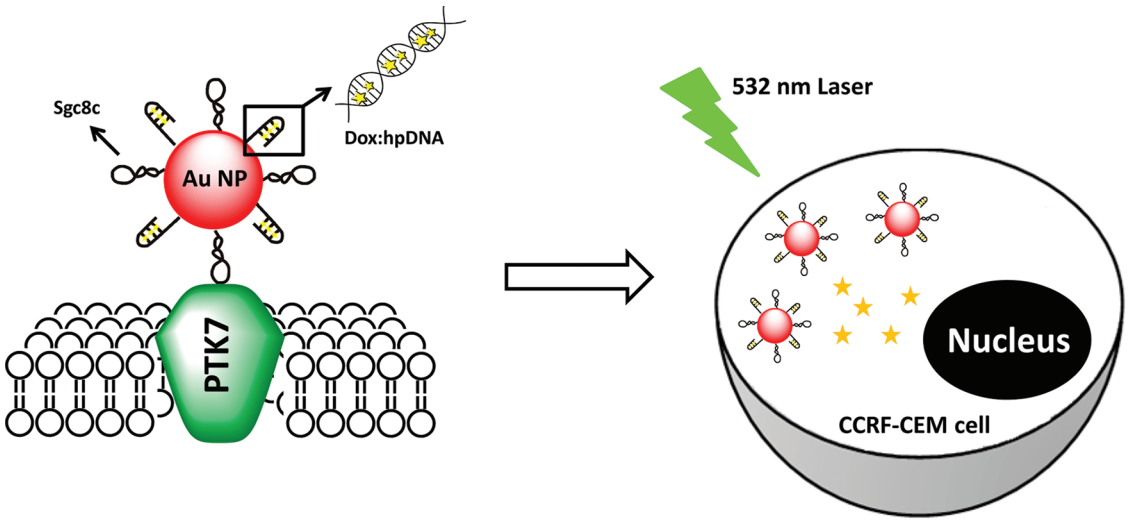

Scheme 1. Light-induced Dox release from Dox:apt/hp-Au NP nanocomplexes inside targeted cancer cells (schematic).

hpDNA onto the surface of Au NPs greatly increases their stability in physiological environments. Moreover, various guest molecules can interact with DNA through intercalation or by binding in the major or minor groove of the double-helix structure.[54−56] Therefore, our hpDNA-conjugated Au NP (hp-Au NPs) nanocomplexes can serve as an effective host for many guest molecules *via* noncovalent interactions. Doxorubicin (Dox), the most utilized anticancer drug against a range of neoplasms, including acute lymphoblastic and myeloblastic leukemias as well as malignant lymphomas,[57] was chosen in this study. Dox binds preferentially to DNA through intercalation between adjacent base pairs; its association with DNA is reversible. Upon illumination with a continuous-wave (CW) laser, corresponding to the resonant wavelength of Au NPs, the input photoenergy and the accompanying local photothermal heating response assist the release of Dox molecules from the Dox-loaded drug carrier, hp-Au NP (Dox:hp-Au NP). These Au NP-based nanocomplexes provide an ideal platform for light-controlled drug delivery in cancer therapy (Scheme 1).

RESULTS AND DISCUSSION

Construction of Dox-Loaded hp-Au NP Conjugates. To demonstrate that photothermal conversion could be used for controllable drug release, hairpin DNA (hpDNA) was utilized as a thermosensitive drug carrier to encapsulate the anticancer reagent doxorubicin (Dox). Considering that Dox preferentially binds to regions rich with cytosine (C) and guanine (G) nucleosides,[58] we designed a six base-pair repeating (CGATCG) sequence with consecutive C-G base pairs to bind as many Dox molecules as possible. Multiple hpDNA was further assembled onto the gold nanoparticle (Au NP) surface to accommodate a high level of drug loading. With precisely controllable density and covalent conjugation, the binding of hpDNA onto the surface of Au NPs greatly increases their stability in physiological environments. Spectrophotometric analysis revealed only a slight change in the NPs' peak absorbance after suspension in saline, confirming successful retention of Au NP stability using thiolated hpDNA (Figure S1 in the Supporting Information). The diameter of citrate-stabilized Au NPs was 12.9 ± 0.3 nm determined by dynamic light scattering (Zetasizer Nano, Malvern Instruments, United Kingdom). After immobilization of hpDNA, the size of the conjugates increased to 18.2 ± 1.6 nm and was further increased to 21.0 ± 1.6 nm by subsequent loading of Dox molecules. This result was in good agreement with the data obtained from ζ-potential measurement. The hpDNA-conjugated Au NPs show a more negative ζ-potential (−48.7 ± 1.7) than do the citrate-stabilized Au NPs (−37.8 ± 1.9). Furthermore, the deposition of Dox molecules leads to a decline in the negative intensity of ζ-potential (−34.7 ± 1.1 mV). These results suggest that hpDNA and Dox were sequentially introduced onto the surface of Au NPs.

The amount of Dox loaded onto each NP was determined indirectly by measuring the fluorescence signal of the removed molecules from Dox:hp-Au NP conjugates through serial washing/centrifugation steps. By fitting the nonlinear regression equation from the Scatchard analysis at various concentrations of free (unbound) Dox, the quantified saturation number was 305 (±9) Dox molecules per NP (Figure 1A). Each NP possessed 83 (±6) hpDNA, and our result suggested that ~4 Dox molecules were bound by each hairpin. The Hill plot displayed in Figure 1B also exhibited fluorescence quenching of Dox as a function of increasing hp-Au NP concentration. The dissociation constant (K_d = 1.2 ± 0.1 nM) derived from this result

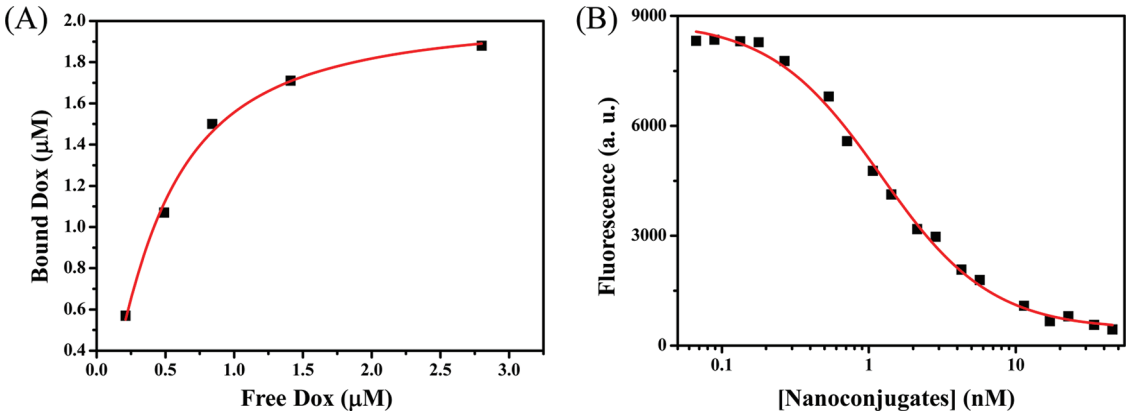

Figure 1. (A) Dox loading analyses of hp-Au NPs. The saturation curve was obtained by exposing different hp-Au NPs (6.7 nM) to 0.8−5.0 μM Dox. The suspension was cleared of unbound Dox by centrifugation (twice). Approximately 305 (±9) Dox molecules were bound on each hp-Au NP. (B) Hill plot for the hp-Au NPs titration (K_d = 1.2 ± 0.1 nM). The fluorescence signals of Dox (1.5 μM) were monitored at 590 nm. Buffer: 10 mM phosphate buffer, 100 mM NaCl, pH 7.4.

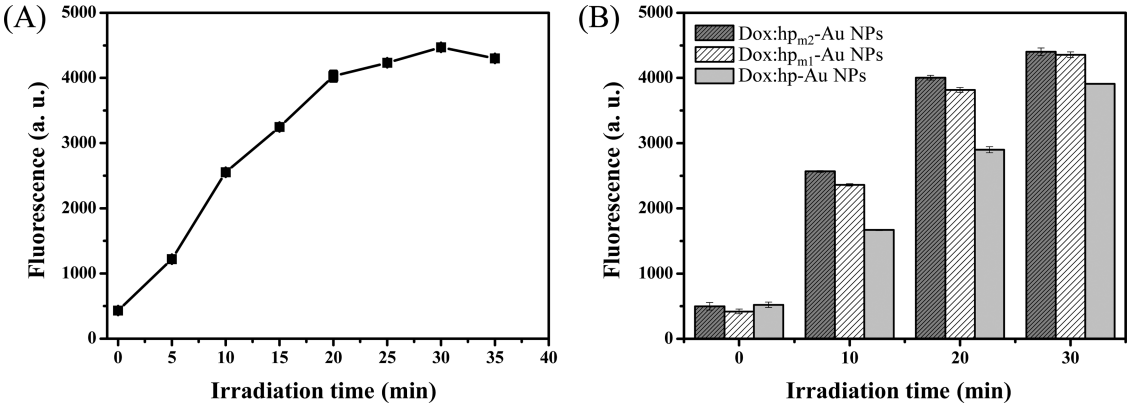

Figure 2. Light-induced Dox release from Dox-loaded hpDNA-modified Au NP conjugates. (A) A solution of Dox:hp-Au NP conjugates was irradiated with visible light (532 nm) for 35 min. The release kinetics of Dox from nanoconjugates to buffer solution (DPBS, 9.6 mM phosphate buffer, 136.8 mM NaCl, 4.2 mM KCl, pH 7.4) was monitored using the fluorescence signal (590 nm) of Dox in the supernatant at each interval after centrifuging down the nanoconjugates. (B) Comparison of the light-induced Dox release from three different Dox-loaded hpDNA-Au NP conjugates at 0, 10, 20, and 30 min.

indicated that a stable Dox:hp-Au NP physical (noncovalent) conjugate was successfully constructed.

The stability of the Dox:hp-Au NP conjugate was further confirmed by dialysis. The complex solution (100 μL) was transferred to dialysis vials (3000 Da cutoff; Pierce, Rockford, IL, USA) and dialyzed against 1% bovine serum albumin/phosphate-buffered saline (BSA/PBS) (10 mM phosphate buffer, 100 mM sodium chloride, pH 7.4) at ambient temperature. Buffer solution outside the dialysis vials was then taken for fluorescence measurement at selected time intervals. Concurrently, free Dox (2.5 μM) was dialyzed under the same condition as the control. Thereafter, the releasing percentage of Dox from the Dox:hp-Au NP physical conjugate over time could be calculated on the basis of the fluorescence intensity at 590 nm. Less than 35(±2)% Dox release was observed in 6 h under vigorous stirring. This suggested that only a small proportion of Dox molecules were liberated from the conjugate by simple diffusion (Figure S2 in the Supporting Information).

Light-Activated Drug Release. To achieve light-activated molecular release, Dox:hp-Au NP complex solution was illuminated with a green CW laser (532 nm) at 2.0 W/cm^2 for different periods. After exposure to laser beams, the supernatants of the sample solution were isolated by centrifugation. The release profile of Dox molecules was quantified by monitoring the increasing fluorescence signals at fixed time intervals (Figure 2A). Without laser irradiation, slight leakage of Dox molecules (<1% of the entire payload) was monitored for the first 35 min. This result further confirmed the stable noncovalent interaction between Dox and the hairpin structures of DNA-conjugated Au NPs. While the suspension was exposed to a green laser, gradual release of Dox molecules was observed within 20 min. The payload leveled off with prolonged irradiation (35 min), which demonstrated after 20 min of laser irradiation that no additional dehybridization of hpDNA occurred.

Although a lack of temperature increase (<2.2 °C) of the ambient suspension was observed after 35 min of irradiation, the light-induced drug release was ascribed to the rapid dehybridization of the hpDNA on the Au NP surface when illuminated with plasmon-resonant light. One possible reason is that the irradiated NP undergoes a rapid and significant temperature increase at its surface sufficient to melt the hpDNA, but this temperature increase is not sufficient to raise the solution temperature.[28] To assess if the light-triggered-releasing effect was temperature dependent, two additional hairpin DNA molecules, hp_{m1} and hp_{m2}, with consistent (CGATCG) binding domains similar to hpDNA but inserted with three and six mismatched base pairs, respectively, were immobilized onto the Au NP surface and incubated with Dox molecules. The loading amount of Dox for these three hpDNA-Au NP conjugates was optimized virtually identically (<3%). When illuminated with a laser (532 nm) at 2.0 W/cm^2 for different periods, an increase in the fluorescence signal was observed for Dox-loaded hpDNA-Au NP conjugates with more mismatched base-pair regions. Specifically, when exposed to 10 min irradiation, the fluorescence signal detected from the released Dox molecules of (drug loaded) − (hp_{m2}-Au NP) and (hp_{m1}-Au NP) conjugates was about 1.5-fold and 1.4-fold stronger than that of Dox:hp-Au NP conjugates, respectively (Figure 2B). This result confirmed that the release profile was temperature dependent, whereas the melting temperature of hp_{m2}, hp_{m1}, and hp was 67.5, 72.3, and 85.9 °C, respectively. The property of thermally induced drug release was also confirmed by immersing the nanocomplex solution in a thermal bath at 80 °C, and the increase of fluorescence signal of released Dox molecules in the supernatant further supported the idea that our hpDNA-Au NP conjugates was temperature-dependent and thermosensitive (Figure S3 in Supporting Information).

Specific Targeting. Targeted delivery to specific cells is essential in chemotherapy. Hence, the aptamer sgc8c, selective to CCRF-CEM cells (T-cell acute lymphoblastic leukemia cell line),[59] was tethered to Dox:hp-Au NP conjugates through a gold−thiol linkage. Aptamers are RNA or DNA molecules that fold by intramolecular interaction into unique three-dimensional conformations for target recognition. They can be selected by SELEX (systematic evolution of ligands by exponential enrichment)[60,61] from a pool of DNA or RNA by repetitive binding of target molecules. Aptamers are highly specific for different types of tumor cells and have excellent binding affinity. They also provide advantageous characteristics, including small size, ease of synthesis and modification, low toxicity or immunogenicity, and high stability. They have therefore emerged as a novel class of molecular probes in diagnostic and therapeutic applications.[62−66] The cellular targeting efficacy of our sgc8c-conjugated hp-Au NP (sgc8c/hp-Au NP) complex was investigated using

a simple competition assay. CCRF-CEM (target) cells were first incubated with sgc8c/hp-Au NPs at 4 °C for 20 min and then labeled with a fluorescein-modified sgc8c. Fluorescence intensity was ultimately determined by flow cytometry. Compared with the conjugates lacking sgc8c, the observation that less fluorescence was detected from CCRF-CEM cells incubated with sgc8c/hp-Au NPs confirmed that the binding sites had already been saturated and that the binding between sgc8c/hp-Au NPs toward CCRF-CEM cells was through the specific binding of sgc8c to its target (Figure 3A). In addition, the binding affinity (K_d) of the sgc8c/hp-Au NP conjugate was determined to be 1.6 (±0.2) nM through an indirect fluorescence measurement (Figure S4 in the Supporting Information). The comparable binding affinity between sgc8c-conjugated nanocomplexes and free sgc8c ($K_d \approx 1$ nM)[67] suggests that the attachment of Au NP to sgc8c had no or little effect on the ability of the aptamer to bind to CCRF-CEM cells.

Similar results were obtained by atomic absorption spectrometry (AAS; AAnalyst 600; PerkinElmer, Waltham, MA, USA) for CCRF-CEM cells incubated with sgc8c/hp-Au NP conjugates at 37 °C for 2 h. After multiple centrifugation/washing cycles, we use trypsin to remove surface-bound particles. The number of sgc8c/hp-Au NPs taken up by CCRF-CEM cells was then evaluated. Figure 3B shows that the maximum number of sgc8c/hp-Au NPs in/on a target cell was 5300 (±128), and <1400 (±67) hp-Au NPs were determined for nonspecific intracellular uptake. In agreement with flow cytometric analyses, sgc8c/hp-Au NPs exhibited remarkable cellular affinity toward CCRF-CEM cells. Our AAS results further confirmed that the uptake of sgc8c/hp-Au NPs toward targeted cells *via* a receptor-mediated process was more efficient than conjugates that lacked the targeting moiety sgc8c.

Selective Toxicity. To assess the tumoricidal potential of our developed targeted drug delivery system, the cytotoxicity of the chemotherapeutic agent utilized in this study, Dox, was first investigated for two leukemia cell lines. Cells that expressed different target proteins of sgc8c were incubated with Dox in culture medium without FBS at 37 °C in an atmosphere of 5% CO_2. After 2 h, unbound Dox molecules were removed by centrifugation and fresh medium (10% FBS) was added for further cell growth (48 h). The relative viability of cells with different treatments was determined by 3-(4,5-dimethylthiazol-2-yl)-5-(3-carboxymethoxyphenyl)-2-(4-sulfophenyl)-2*H*-tetrazolium) (MTT) assay. The results shown in Figure 4 demonstrated that Dox at micromolar levels possessed high toxicity toward CCRF-CEM and Ramos cells and could greatly inhibit

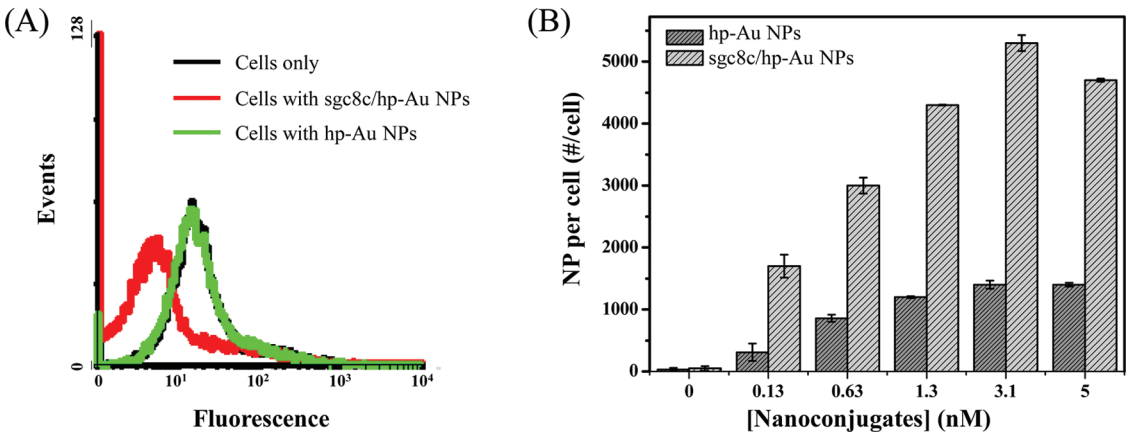

Figure 3. (A) Flow cytometric assay for the binding of different nanoconjugates with CCRF-CEM cells. The curves represent the fluorescence from fluorescein-sgc8c incubated with pure cells and cells labeled with sgc8c/hp-Au NPs and hp-Au NPs (3.4 nM). The fluorescence is derived from the second stain of cells by fluorescein-labeled sgc8c. (B) Dependence of cellular uptake of different nanoconjugates (sgc8c/hp-Au NPs and hp-Au NPs) as a function of concentration. The concentrations of Au NPs were determined using atomic absorption spectrometry.

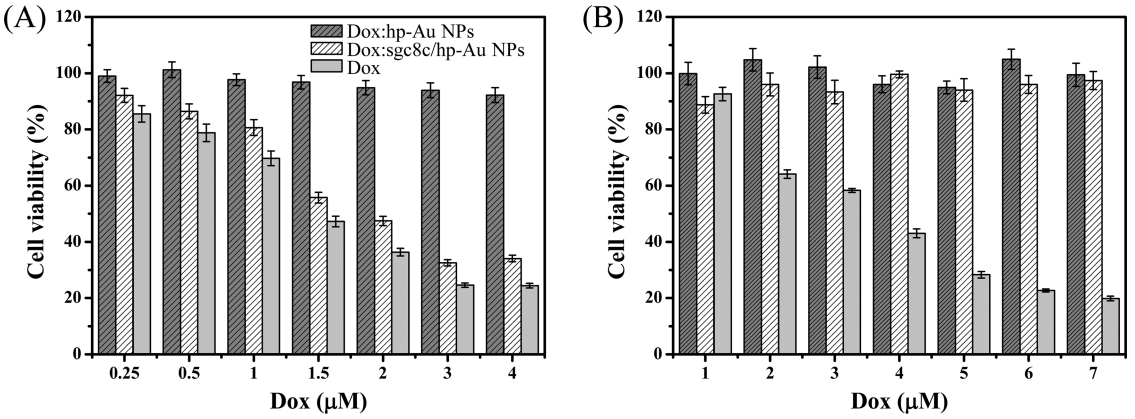

Figure 4. Cytotoxicity assays of (A) CCRF-CEM (target) cells and (B) Ramos (control) cell lines with free Dox, Dox:sgc8c/hp-Au NPs, and Dox:hpDNA-Au NPs. Cells (2×10^4 cells/well) were incubated with Dox or Dox:nanoconjugates (0−5.0 μM) in culture medium without FBS at 37 °C in an atmosphere of 5% CO_2 for 2 h. After drug treatment, cells were grown in fresh medium (10% FBS) for 48 h. Cytotoxicity was measured by the MTT assay.

cell proliferation.[57] However, the cytotoxic effect of Dox:hp-Au NPs toward CCRF-CEM (target) cells and Ramos (control) cells was <7.8 ± 7.0% and <5.1 ± 2.3%, respectively, indicating that nonspecific uptake of Dox was minimized by the formation of a stable Dox:hp-Au NP physical conjugate. The viability of cells incubated with hp-Au NP was also compared with that of untreated cells. Only 5.2 (±6.8)% of CEM cells and 4.0 (±9.8)% of Ramos cells were killed. This supported the idea that the hp-Au NP nanocomplex (12.6 nM) shows little or no toxicity to cells (data not shown).

Specific killing efficiency was also investigated by incubating target cells with Dox-loaded hp-Au NPs, which had been conjugated with sgc8c. Dox:sgc8c/hp AuNPs can bind specifically to protein tyrosine kinase 7 (PTK7)-abundant CCRF-CEM cells.[67] Figure 4A demonstrates that the inhibition concentration (IC_{50}) of Dox:sgc8c/hp AuNPs was 1.4 ± 0.1 μM, which is quite similar to that for free Dox (IC_{50} = 1.3 ± 0.1 μM) (Figure S5 in the Supporting Information). This comparative study provided strong evidence that, whereas hp-Au NP showed limited internalization, our sgc8c-conjugated drug nanocarrier could recognize and be taken up by its target cells specifically. Nontargeted Ramos (control) cells were tested with the binding of Dox-loaded sgc8c/hp-Au NPs under identical experimental conditions. In contrast to the dramatic cytotoxic effect of Dox:nanoconjugates to CCRF-CEM cells, the killing efficacy of Dox:sgc8c/hp-Au NPs toward Ramos cells was significantly less pronounced. This was attributed to the lack of PTK7 expression on the surface of Ramos cells.

Having established that the constructed drug release system was light-controllable, we next investigated the cytotoxic effect induced by laser irradiation. CCRF-CEM cells were incubated with different conjugates and then exposed to 532 nm laser illumination

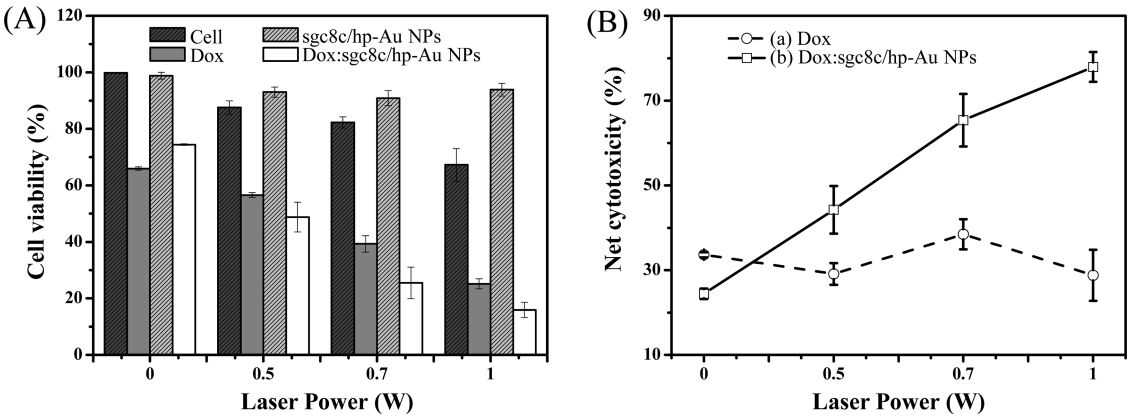

Figure 5. (A) Cytotoxicity assays of CCRF-CEM (target) cell lines and those incubated with free Dox, sgc8c/hp-Au NPs, and Dox:sgc8/hp-Au NPs. (B) The net cytotoxicity (%) represents the different values of cell viability (%) for (a) cells incubated with Dox relative to untreated cells and (b) cells incubated with Dox:sgc8c/hp-Au NPs, in comparison with sgc8c/hp-Au NP-labeled cells. Cells were exposed to a green laser at 532 nm at different laser power (0, 1.0, 1.4, and 2.0 W/cm^2) for 10 min. After treatment, cells were grown in fresh medium (10% FBS) for 48 h. Cytotoxicity was measured by the MTT assay.

for 10 min at 0.5, 0.7, and 1.0 W. The first column in Figure 5A demonstrates that CCRF-CEM cells were susceptible to light-induced cellular damage. However, cells that had been labeled with sgc8c/hp-Au NPs and then irradiated (2.0 W/cm^2, 10 min) maintained a high proliferation rate (93.9 ($\pm$4.5)%) by MTT measurement. Observation of a less pronounced cytotoxic effect of cells incubated with sgc8c/hp-Au NPs suggested an inner-filter effect of Au NPs in/on CCRF-CEM cells. Cells were, therefore, less susceptible to photoinduced damage. The different values of cytotoxicity between Dox:sgc8c/hp-Au NPs and sgc8c/hp-Au NPs (denoted as squares in Figure 5B) were further compared with that of free Dox relative to untreated cells (denoted as circles in Figure 5B). There was no apparent tendency that the differences in cellular response (dashed line a) increased or decreased under different power of laser exposure. On the contrary, as the laser power increased, the solid line (b) in Figure 5B demonstrated a greater potency of Dox:sgc8c/hp-Au NPs in comparison with sgc8c/hp-Au NPs. These results are consistent with a mechanism whereby Au NPs absorb laser light, convert it to heat, and then dissipate heat energy to the surroundings, leading to a gradual release of Dox molecules.

The effectiveness of light-induced intracellular Dox release was further investigated by flow cytometry (Figure S6 in the Supporting Information). The fluorescence signal of Dox molecules from each cell suspension was determined. The irradiation time, as well as the laser power level, was optimized by repeated experiments to achieve the best performance. Evidence of Dox release was demonstrated by the increase in fluorescence intensity after laser treatment (65.3 $\pm$ 4.8) from cells incubated with Dox:hp/sgc8c-Au NPs compared with that before irradiation (28.5 $\pm$ 2.5) (Figure S6A). Au NP can quench the fluorescence of Dox *via* nonradiative energy transfer and collisional quenching. Hence, the Dox fluorescence observed within cells before light exposure arose from those noncontrollably released from the complexes after cellular uptake. The 229% increase in Dox fluorescence after laser treatment indicated that light was crucial to trigger an effective release of guest molecules from the host carriers, hp DNA-conjugated Au NPs, inside the cells. Conversely, a control experiment involving CCRF-CEM cells incubated with free Dox molecules demonstrated no statistically significant increase in Dox fluorescence after laser irradiation (33.6 $\pm$ 0.1 to 31.2 $\pm$ 2.7) (Figure S6B). Fluorescence images of CCRF-CEM cells incubated with Dox:hp/sgc8c-Au NPs show visually an increasing brightness in Dox fluorescence inside cells after laser treatment, whereas no obvious fluorescence signal change was observed for Dox-treated cells. This result further confirmed that the enhanced cellular toxicity toward targeted cells incubated with Dox:hp/sgc8c-Au NPs originated from the greater-releasing Dox molecules inside cells after illumination of plasmon-resonant light.

CONCLUSIONS

We successfully developed a light-responsive drug delivery platform based on Au NPs coated with a dense monolayer of hpDNA. Multiple copies of therapeutic reagents and Dox molecules can bind reversibly to the double-helix structures on the NP surface. The constructed nanoconjugates, therefore, accommodate a high level of drug loading. These nanoconjugates can also be readily functionalized with targeting moieties (*e.g.*, aptamers) for specific recognition of tumor cells. When exposed to laser illumination, the photothermal effect of Au NPs leads to rapid dissipation of heat into the surroundings, thereby triggering the release of encapsulated molecules with high controllability. The *in vitro* study

confirmed that linking cell-SELEX-selected aptamers with our novel drug nanocarriers is feasible for targeted drug delivery and that remote-control capability with light illumination also shows their potential effectiveness and flexibility in the precise release of drugs.

EXPERIMENTAL DETAILS

Chemicals. Sodium tetrachloroaurate(III) dihydrate (99%), Tris, doxorubicin, 6-mercapto-1-hexanol, (97%), trisodium citrate 2-hydrate, and sodium chloride were obtained from Sigma-Aldrich (St. Louis, MO, USA). Fetal bovine serum and penicillin/streptomycin were obtained from Gibco (Grand Island, NY, USA). Dulbecco's phosphate-buffered saline was purchased from Biosource (Camarillo, CA, USA). The 5′-thiol-modified aptamer (sgc8c, 5′-thiol-ATC TAA CTG CTG CGC CGC CGG GAA AAT ACT GTA CGG TTA GA), hairpin DNA (hp, 5′-thiol-TTT TTT TTT TCG ATC GCG ATC GCG ATC GTT TTC GAT CGC GAT CGC GAT CG), hp_{m1} (5′-thiol-TTT TTT TTT TCG ATC GTC GAT CGT CGA TCG TTT TCG ATC GTC GAT CGT CGA TCG), and hp_{m2} (5′-thiol-TTT TTT TTT TCG ATC GTT CGA TCG TTC GAT CGT TTT CGA TCG TTC GAT CGT TCG ATC G) were purchased from Integrated DNA Technology Incorporated (Coralville, IA, USA). Deionized water (18.2 MΩ·cm) was used to prepare all of the aqueous solutions. For the cellular experiments, all of the reagents, buffers, and culture medium were sterilized by steam autoclave (121 °C, 15 min) or filtration (0.22 μm pore size, Millipore) and maintained under sterile conditions.

Synthesis of Au NPs. Au NPs were synthesized according to the method developed by Frens.[68] Briefly, 0.1 mL of 1.0 M chloroauric acid was added to 100 mL of deionized water, and the solution boiled. Next, 1.0 mL of 0.4 M trisodium citrate was added to the solution to obtain 12.6 (±0.8) nm AuNPs (Figure S1D in the Supporting Information). The solution was refluxed until a color change from dark blue to red. The sizes and absorption spectra of Au NPs were verified using a Hitachi H-7100 transmission electron microscope (Tokyo, Japan) and a Cary 100 UV−vis spectrophotometer (Varian, Palo Alto, CA, USA). The concentration of Au NPs in each aliquot was also determined by UV−vis spectrophotometic measurements *via* Beer's law ($A = \varepsilon bc$).[69] The concentration of the as-prepared Au NP solutions was 13.0 nM.

Synthesis of Drug-Loaded Nanoconjugates. Hairpin DNA (hpDNA) was reacted directly with Au NPs through attachment of mercaptohexanol and oligo-S units onto the Au NP surface; the bioconjugate was denoted "hp-Au NP". Briefly, a 200 μL aliquot of aqueous Au NP solution was mixed with 2.8 μL of 100 μM hpDNA to obtain a final concentration of 12.6 nM hp-Au NPs. After reaction for 12 h at room temperature, 2.0 M NaCl was added to bring the salt concentration to 0.1 M. This solution was incubated for an additional 12 h. Next, the mixture was equilibrated with 0.8 μL of 1.0 mM 6-mercaptohexanol for 30 min before conducting two centrifuge/wash cycles (18 000 rpm, 15 min) to remove excess hpDNA. hp-Au NPs were resuspended in an aqueous solution of Dox (4.5 μM), incubated for 2 h, and centrifuged at 18 000 rpm for 15 min to remove excess Dox. The amount of unbound Dox molecules in the supernatant was calculated from the emission intensity of Dox at 590 nm (excitation at 480 nm). For the construction of sgc8c/hp-Au NPs: after removing unreacted hpDNA, hp-Au NPs solution was equilibrated with 5′-thiol-modified sgc8c (0.56 μM) in phosphate buffer saline (10 mM phosphate, 100 mM NaCl, pH 7.4). After reaction for 15 min, the concentration of salt was increased to 0.2 M using 2.0 M NaCl, followed by 20 min incubation period at room temperature. The salt aging process was repeated for every 0.1 M NaCl increment thereafter until a concentration of 0.7 M NaCl was reached. After overnight incubation, the mixture was equilibrated with 0.8 μL of 1.0 mM 6-mercaptohexanol for 30 min followed by two centrifuge/wash cycles (18 000 rpm, 15 min) to remove unreacted sgc8c.

Characterization of DNA Loading. The loading of DNA onto the Au NP surface was determined by fluorescence measurement (Tecan Safire Plate Reader, Tecan Group AG, Basel, Switzerland) of fluorescein-labeled oligonucleotides. The fluorescence maxima (measured at 520 nm) of the supernatant, containing free oligonucleotides removed from the particle, were converted to molar concentrations of fluorescein-alkanethiol-modified DNA by interpolation from a standard linear calibration curve. Standard curves were prepared with known concentrations of fluorescein-labeled oligonucleotides using identical buffer pH and salt concentrations. Finally, the mean number of oligonucleotides per particle was obtained by dividing the measured oligonucleotide molar concentration by the original Au NP concentration.

Cell Lines and Buffers. CCRF-CEM cells (CCL-119 T-cell, human acute lymphoblastic leukemia) and Ramos cells (CRL-1596, B-cell, human Burkitt's lymphoma) were obtained from American Type Culture Collection (ATCC; Manassas, VA, USA). Cells were cultured in RPMI medium supplemented with 10% fetal bovine serum and 1% penicillin−streptomycin (Invitrogen, Carlsbad, CA, USA). Cell density was determined using a hemocytometer, and this was done before experimentation. One million cells dispersed in washing buffer [4.5 g/L glucose and 5 mM $MgCl_2$ in Dulbecco's PBS with calcium chloride and magnesium chloride (Sigma−Aldrich)] were centrifuged at 1000 rpm for 5 min and redispersed in the same buffer for incubation. During experiments, cells were kept in an ice bath at 4 °C.

Flow Cytometric Analyses. The binding affinity of sgc8c/hp-Au NP conjugate was determined by incubating CCRF-CEM cells (10^6) on ice for 20 min with a serial concentration of sgc8c/hp-Au NP conjugates in 0.1 mL washing buffer (containing 1% BSA). Cells were washed twice with washing buffer (0.5 mL) and suspended in fluorescein-labeled sgc8c (25 nM, 0.1 mL) for further incubation (20 min on ice). Before flow cytometric analyses (BD FACSCanto, BD Bioscience, Franklin Lakes, NJ, USA), cells were washed with washing buffer and then reacted with trypsin (500 μL, 0.05%)/EDTA (0.53 mM) in HBSS at 37 °C for 10 min. After the incubation, FBS (50 μL) was added, and the cells were again washed with the washing buffer (500 μL) and suspended in washing buffer (0.2 mL). The mean fluorescence intensity of cells labeled with fluorescein-sgc8c was used to calculate the equilibrium dissociation constant (K_d) of the interaction of sgc8c/hp-Au NP and CCRF-CEM cells by fitting the dependence of fluorescence intensity (F) on the concentration of the apt/hp-Au NP (L) to the equation $F = B_{max}[L]/(K_d + [L])$. The binding assay experiments were repeated at least three times.

Cytotoxicity Assay. Chemosensitivity of cell lines to Dox or Dox-loaded nanoconjugates was determined using the Cell Titer 96 cell proliferation assay (Promega, Madison, WI, USA). Cells (2×10^4 cells/well) were incubated with Dox or Dox-loaded nanoconjugates (0−4 μM) in culture medium without FBS at 37 °C in an atmosphere of 5% CO_2. After 2 h, 75% of media was removed and fresh media (10% FBS) added for further cell growth (48 h). For cytotoxicity measurement, Cell Titer reagent (10 μL) was added to each well and incubated for 2 h. Using a plate reader (Tecan Safire), the absorption was recorded at 570 and 600 nm. The percentage of cell viability was determined by comparing cells treated with Dox and Dox-loaded nanoconjugates with the untreated control.

Acknowledgment. This work was supported by National Tsing Hua University (99N2947E1, 99N82531E1) and the National Science Council (98-2113-M-007-003, 99-2113-M-007-006-MY2, 99-2627-M-007-010) of Taiwan, ROC.

Supporting Information Available: Supplementary figures including UV−vis absorption spectra, hydrodynamic size distribution, zeta potential, TEM images, flow cytometric histograms, and microscopic images are available free of charge *via* the Internet (http://pubs.acs.org).

REFERENCES AND NOTES

1. Bajpai, A. K.; Shukla, S. K.; Bhanu, S.; Kankane, S. Responsive Polymers in Controlled Drug Delivery. *Prog. Polym. Sci.* **2008**, *33*, 1088–1118.
2. Kim, T.; Huh, Y. M.; Haam, S.; Lee, K. Activatable Nanomaterials at the Forefront of Biomedical Sciences. *J. Mater. Chem.* **2010**, *20*, 8194–8206.
3. Ganta, S.; Devalapally, H.; Shahiwala, A.; Amiji, M. A Review of Stimuli-Responsive Nanocarriers for Drug and Gene Delivery. *J. Controlled Release* **2008**, *126*, 187–204.
4. Du, F.-S.; Wang, Y.; Zhang, R.; Li, Z.-C. Intelligent Nucleic Acid Delivery Systems Based on Stimuli-Responsive Polymers. *Soft Matter* **2010**, *6*, 835–848.
5. Soliman, M.; Allen, S.; Davies, M. C.; Alexander, C. Responsive Polyelectrolyte Complexes for Triggered Release of Nucleic Acid Therapeutics. *Chem. Commun.* **2010**, *46*, 5421–5433.
6. Chung, H. J.; Park, T. G. Self-Assembled and Nanostructured Hydrogels for Drug Delivery and Tissue Engineering. *Nano Today* **2009**, *4*, 429–437.
7. Stuart, M. A. C.; Huck, W. T. S.; Genzer, J.; Muller, M.; Ober, C.; Stamm, M.; Sukhorukov, G. B.; Szleifer, I.; Tsukruk, V. V.; Urban, M.; *et al.* Emerging Applications of Stimuli-Responsive Polymer Materials. *Nat. Mater.* **2010**, *9*, 101–113.
8. Chilkoti, A.; Dreher, M. R.; Meyer, D. E.; Raucher, D. Targeted Drug Delivery by Thermally Responsive Polymers. *Adv. Drug Delivery Rev.* **2002**, *54*, 613–630.
9. Nakayama, M.; Okano, T.; Miyazaki, T.; Kohori, F.; Sakai, K.; Yokoyama, M. Molecular Design of Biodegradable Polymeric Micelles for Temperature-Responsive Drug Release. *J. Controlled Release* **2006**, *115*, 46–56.
10. Klouda, L.; Mikos, A. G. Thermoresponsive Hydrogels in Biomedical Applications. *Eur. J. Pharm. Biopharm.* **2008**, *68*, 34–45.
11. Lyon, L. A.; Meng, Z.; Singh, N.; Sorrell, C. D., St.; John, A. Thermoresponsive Microgel-Based Materials. *Chem. Soc. Rev.* **2009**, *38*, 865–874.
12. Rodríguez-Hernández, J.; Chécot, F.; Gnanou, Y.; Lecommandoux, S. Toward 'Smart' Nano-Objects by Self-Assembly of Block Copolymers in Solution. *Prog. Polym. Sci.* **2005**, *30*, 691–724.
13. Slowing, I. I.; Vivero-Escoto, J. L.; Wu, C.-W.; Lin, V. S. Y. Mesoporous Silica Nanoparticles as Controlled Release Drug Delivery and Gene Transfection Carriers. *Adv. Drug Delivery Rev.* **2008**, *60*, 1278–1288.
14. Gao, W. W.; Chan, J. M.; Farokhzad, O. C. pH-Responsive Nanoparticles for Drug Delivery. *Mol. Pharmaceutics* **2010**, *7*, 1913–1920.
15. Casasús, R.; Climent, E.; Marcos, M. D.; Martónez-Máñez, R.; Sancenón, F.; Soto, J.; Amorós, P.; Cano, J.; Ruiz, E. Dual Aperture Control on pH- and Anion-Driven Supramolecular Nanoscopic Hybrid Gate-like Ensembles. *J. Am. Chem. Soc.* **2008**, *130*, 1903–1917.
16. Guiseppi-Elie, A. Electroconductive Hydrogels: Synthesis, Characterization and Biomedical Applications. *Biomaterials* **2010**, *31*, 2701–2716.
17. De, M.; Ghosh, P. S.; Rotello, V. M. Applications of Nanoparticles in Biology. *Adv. Mater.* **2008**, *20*, 4225–4241.
18. Lu, Z.-R.; Kopečková, P.; Kopeček, J. Antigen Responsive Hydrogels Based on Polymerizable Antibody Fab′ Fragment. *Macromol. Biosci.* **2003**, *3*, 296–300.
19. Miyata, T.; Jige, M.; Nakaminami, T.; Uragami, T. Tumor Marker-Responsive Behavior of Gels Prepared by Biomolecular Imprinting. *Proc. Natl. Acad. Sci.U. S. A.* **2006**, *103*, 1190–1193.
20. Law, B.; Tung, C.-H. Proteolysis: A Biological Process Adapted in Drug Delivery, Therapy, and Imaging. *Bioconjugate Chem.* **2009**, *20*, 1683–1695.
21. Schlossbauer, A.; Kecht, J.; Bein, T. Biotin−Avidin as a Protease-Responsive Cap System for Controlled Guest Release from Colloidal Mesoporous Silica. *Angew. Chem., Int. Ed.* **2009**, *48*, 3092–3095.
22. Gil, E. S.; Hudson, S. M. Stimuli-Reponsive Polymers and Their Bioconjugates. *Prog. Polym. Sci.* **2004**, *29*, 1173–1222.
23. Alarcón, C. d. l. H.; Pennadam, S.; Alexander, C. Stimuli Responsive Polymers for Biomedical Applications. *Chem. Soc. Rev.* **2005**, *34*, 276–285.
24. Gupta, P.; Vermani, K.; Garg, S. Hydrogels: from Controlled Release to pH-Responsive Drug Delivery. *Drug Discovery Today* **2002**, *7*, 569–579.
25. Chaterji, S.; Kwon, I. K.; Park, K. Smart Polymeric Gels: Redefining the Limits of Biomedical Devices. *Prog. Polym. Sci.* **2007**, *32*, 1083–1122.
26. Derfus, A. M.; von Maltzahn, G.; Harris, T. J.; Duza, T.; Vecchio, K. S.; Ruoslahti, E.; Bhatia, S. N. Remotely Triggered Release from Magnetic Nanoparticles. *Adv. Mater.* **2007**, *19*, 3932−+.
27. Aznar, E.; Marcos, M. D.; Martínez-Máñez, R. n.; Sancenón, F. l.; Soto, J.; Amorós, P.; Guillem, C. pH- and Photo-Switched Release of Guest Molecules from Mesoporous Silica Supports. *J. Am. Chem. Soc.* **2009**, *131*, 6833–6843.
28. Barhoumi, A.; Huschka, R.; Bardhan, R.; Knight, M. W.; Halas, N. J. Light-Induced Release of DNA from Plasmon-Resonant Nanoparticles: Towards Light-Controlled Gene Therapy. *Chem. Phys. Lett.* **2009**, *482*, 171–179.
29. Yavuz, M. S.; Cheng, Y.; Chen, J.; Cobley, C. M.; Zhang, Q.; Rycenga, M.; Xie, J.; Kim, C.; Song, K. H.; Schwartz, A. G. *et al.* Gold Nanocages Covered by Smart Polymers for Controlled Release with Near-Infrared Light. *Nat. Mater.* **2009**, *8*, 935–939.
30. Satarkar, N. S.; Biswal, D.; Hilt, J. Z. Hydrogel Nanocomposites: A Review of Applications as Remote Controlled Biomaterials. *Soft Matter* **2010**, *6*, 2364–2371.
31. Timko, B. P.; Dvir, T.; Kohane, D. S. Remotely Triggerable Drug Delivery Systems. *Adv. Mater.* **2010**, *22*, 4925–4943.
32. Rai, P.; Mallidi, S.; Zheng, X.; Rahmanzadeh, R.; Mir, Y.; Elrington, S.; Khurshid, A.; Hasan, T. Development and Applications of Photo-Triggered Theranostic Agents. *Adv. Drug Delivery Rev.* **2010**, *62*, 1094–1124.
33. Medeiros, S. F.; Santos, A. M.; Fessi, H.; Elaissari, A. Stimuli-Responsive Magnetic Particles for Biomedical Applications. *Int. J. Pharm.* **2011**, *403*, 139–161.
34. Jain, P. K.; Huang, X.; El-Sayed, I. H.; El-Sayed, M. A. Noble Metals on the Nanoscale: Optical and Photothermal Properties and Some Applications in Imaging, Sensing, Biology, and Medicine. *Acc. Chem. Res.* **2008**, *41*, 1578–1586.
35. Richardson, H. H.; Carlson, M. T.; Tandler, P. J.; Hernandez, P.; Govorov, A. O. Experimental and Theoretical Studies of Light-to-Heat Conversion and Collective Heating Effects in Metal Nanoparticle Solutions. *Nano Lett.* **2009**, *9*, 1139–1146.
36. Colvin, V. L. The Potential Environmental Impact of Engineered Nanomaterials. *Nat. Biotechnol.* **2003**, *21*, 1166–1170.
37. Takahashi, H.; Niidome, Y.; Niidome, T.; Kaneko, K.; Kawasaki, H.; Yamada, S. Modification of Gold Nanorods Using Phosphatidylcholine to Reduce Cytotoxicity. *Langmuir* **2005**, *22*, 2–5.
38. Ding, H.; Yong, K.-T.; Roy, I.; Pudavar, H. E.; Law, W. C.; Bergey, E. J.; Prasad, P. N. Gold Nanorods Coated with Multilayer Polyelectrolyte as Contrast Agents for Multimodal Imaging. *J. Phys. Chem. C* **2007**, *111*, 12552–12557.
39. Fischer, H. C.; Chan, W. C. W. Nanotoxicity: The Growing Need for in Vivo Study. *Curr. Opin. Biotechnol.* **2007**, *18*, 565–571.
40. Murphy, C. J.; Gole, A. M.; Stone, J. W.; Sisco, P. N.; Alkilany, A. M.; Goldsmith, E. C.; Baxter, S. C. Gold Nanoparticles in Biology: Beyond Toxicity to Cellular Imaging. *Acc. Chem. Res.* **2008**, *41*, 1721–1730.
41. Lal, S.; Clare, S. E.; Halas, N. J. Nanoshell-Enabled Photothermal Cancer Therapy: Impending Clinical Impact. *Acc. Chem. Res.* **2008**, *41*, 1842–1851.
42. Huang, X. H.; Neretina, S.; El-Sayed, M. A. Gold Nanorods: From Synthesis and Properties to Biological and Biomedical Applications. *Adv. Mater.* **2009**, *21*, 4880–4910.
43. Murphy, C. J.; Thompson, L. B.; Alkilany, A. M.; Sisco, P. N.; Boulos, S. P.; Sivapalan, S. T.; Yang, J. A.; Chernak, D. J.; Huang, J. Y. The Many Faces of Gold Nanorods. *J. Phys. Chem. Lett.* **2010**, *1*, 2867–2875.

44. Giljohann, D. A.; Seferos, D. S.; Daniel, W. L.; Massich, M. D.; Patel, P. C.; Mirkin, C. A. Gold Nanoparticles for Biology and Medicine. *Angew. Chem., Int. Ed.* **2010**, *49*, 3280–3294.
45. Chen, J. Y.; Yang, M. X.; Zhang, Q. A.; Cho, E. C.; Cobley, C. M.; Kim, C.; Glaus, C.; Wang, L. H. V.; Welch, M. J.; Xia, Y. N.; Gold Nanocages, A Novel Class of Multifunctional Nanomaterials for Theranostic Applications. *Adv. Funct. Mater.* **2010**, *20*, 3684–3694.
46. Chen, C.-C.; Lin, Y.-P.; Wang, C.-W.; Tzeng, H.-C.; Wu, C.-H.; Chen, Y.-C.; Chen, C.-P.; Chen, L.-C.; Wu, Y.-C. DNA-Gold Nanorod Conjugates for Remote Control of Localized Gene Expression by near Infrared Irradiation. *J. Am. Chem. Soc.* **2006**, *128*, 3709–3715.
47. Karg, M.; Pastoriza-Santos, I.; Pérez-Juste, J.; Hellweg, T.; Liz-Marzán, L. M. Nanorod-Coated PNIPAM Microgels: Thermoresponsive Optical Properties. *Small* **2007**, *3*, 1222–1229.
48. Wijaya, A.; Schaffer, S. B.; Pallares, I. G.; Hamad-Schifferli, K. Selective Release of Multiple DNA Oligonucleotides from Gold Nanorods. *ACS Nano* **2008**, *3*, 80–86.
49. Braun, G. B.; Pallaoro, A.; Wu, G.; Missirlis, D.; Zasadzinski, J. A.; Tirrell, M.; Reich, N. O. Laser-Activated Gene Silencing *via* Gold Nanoshell−siRNA Conjugates. *ACS Nano* **2009**, *3*, 2007–2015.
50. Yang, J.; Lee, J.; Kang, J.; Oh, S. J.; Ko, H.-J.; Son, J.-H.; Lee, K.; Suh, J.-S.; Huh, Y.-M.; Haam, S. Smart Drug-Loaded Polymer Gold Nanoshells for Systemic and Localized Therapy of Human Epithelial Cancer. *Adv. Mater.* **2009**, *21*, 4339–4342.
51. Park, H.; Yang, J.; Lee, J.; Haam, S.; Choi, I.-H.; Yoo, K.-H. Multifunctional Nanoparticles for Combined Doxorubicin and Photothermal Treatments. *ACS Nano* **2009**, *3*, 2919–2926.
52. You, J.; Zhang, G.; Li, C. Exceptionally High Payload of Doxorubicin in Hollow Gold Nanospheres for Near-Infrared Light-Triggered Drug Release. *ACS Nano* **2010**, *4*, 1033–1041.
53. Park, J.-H.; von Maltzahn, G.; Xu, M. J.; Fogal, V.; Kotamraju, V. R.; Ruoslahti, E.; Bhatia, S. N.; Sailor, M. J. Cooperative Nanomaterial System to Sensitize, Target, and Treat Tumors. *Proc. Natl. Acad. Sci. U. S. A.* **2010**, *107*, 981–986.
54. Neto, B. A. D.; Lapis, A. A. M. Recent Developments in the Chemistry of Deoxyribonucleic Acid (DNA) Intercalators: Principles, Design, Synthesis, Applications and Trends. *Molecules* **2009**, *14*, 1725–1746.
55. Kim, D.; Jeong, Y. Y.; Jon, S.; Drug-Loaded Aptamer−Gold Nanoparticle, A Bioconjugate for Combined CT Imaging and Therapy of Prostate Cancer. *ACS Nano* **2010**, *4*, 3689–3696.
56. Shieh, Y.-A.; Yang, S.-J.; Wei, M.-F.; Shieh, M.-J. Aptamer-Based Tumor-Targeted Drug Delivery for Photodynamic Therapy. *ACS Nano* **2010**, *4*, 1433–1442.
57. Huang, Y. F.; Shangguan, D. H.; Liu, H. P.; Phillips, J. A.; Zhang, X. L.; Chen, Y.; Tan, W. H. Molecular Assembly of an Aptamer-Drug Conjugate for Targeted Drug Delivery to Tumor Cells. *ChemBioChem* **2009**, *10*, 862–868.
58. Frederick, C. A.; Williams, L. D.; Ughetto, G.; Vandermarel, G. A.; Vanboom, J. H.; Rich, A.; Wang, A. H. J. Structural Comparison of Anticancer Drug DNA Complexes - Adriamycin and Daunomycin. *Biochemistry* **1990**, *29*, 2538–2549.
59. Shangguan, D.; Li, Y.; Tang, Z.; Cao, Z. C.; Chen, H. W.; Mallikaratchy, P.; Sefah, K.; Yang, C. J.; Tan, W. Aptamers Evolved from Live Cells as Effective Molecular Probes for Cancer Study. *Proc. Natl. Acad. Sci. U. S. A.* **2006**, *103*, 11838–11843.
60. Ellington, A. D.; Szostak, J. W. In Vitro Selection of RNA Molecules That Bind Specific Ligands. *Nature* **1990**, *346*, 818–822.
61. Tuerk, C.; Gold, L. Systematic Evolution of Ligands by Exponential Enrichment - RNA Ligands to Bacteriophage-T4 DNA-Polymerase. *Science* **1990**, *249*, 505–510.
62. Levy-Nissenbaum, E.; Radovic-Moreno, A. F.; Wang, A. Z.; Langer, R.; Farokhzad, O. C. Nanotechnology and Aptamers: Applications in Drug Delivery. *Trends Biotechnol.* **2008**, *26*, 442–449.
63. Yan, A. C.; Levy, M. Aptamers and Aptamer Targeted Delivery. *RNA Biol.* **2009**, *6*, 316–320.
64. Thiel, K. W.; Giangrande, P. H. Therapeutic Applications of DNA and RNA Aptamers. *Oligonucleotides* **2009**, *19*, 209–222.
65. Liu, J.; Cao, Z.; Lu, Y. Functional Nucleic Acid Sensors. *Chem. Rev* **2009**, *109*, 1948–1998.
66. Fang, X. H.; Tan, W. H. Aptamers Generated from Cell-SELEX for Molecular Medicine: A Chemical Biology Approach. *Acc. Chem. Res.* **2010**, *43*, 48–57.
67. Shangguan, D.; Cao, Z.; Meng, L.; Mallikaratchy, P.; Sefah, K.; Wang, H.; Li, Y.; Tan, W. Cell-Specific Aptamer Probes for Membrane Protein Elucidation in Cancer Cells. *J. Proteome Res.* **2008**, *7*, 2133–2139.
68. Frens, G. Controlled Nucleation for Regulation of Particle-Size in Monodisperse Gold Suspensions. *Nat. Phys. Sci.* **1973**, *241*, 20–22.
69. Hurst, S. J.; Lytton-Jean, A. K. R.; Mirkin, C. A. Maximizing DNA Loading on a Range of Gold Nanoparticle Sizes. *Anal. Chem.* **2006**, *78*, 8313–8318.